Adaptive Resource Allocation Neural Network-Based Mammogram Image Segmentation and Classification

INDRA P (INDRAgce10004@hotmail.com)
Government College of Engineering
Kavithaa G
Government College of Engineering

Research Article

Keywords: Adaptive Resource Allocation Neural Network, Butterworth filter, histogram equalization, breast cancer

Posted Date: September 22nd, 2021

DOI: https://doi.org/10.21203/rs.3.rs-919373/v1

Adaptive Resource Allocation Neural Network-Based Mammogram Image Segmentation and Classification

[1]P. INDRA, Assistant Professor

[2]Dr.G.Kavithaa, Assistant Professor

[1,2]Department of Electronics and Communication Engineering,

[1,2]Government College of Engineering, Salem, Tamilnadu, India.

Mail ID: [1] INDRAgce10004@hotmail.com, [2]kavi.dhanya@gmail.com

ABSTRACT

Image processing innovations assume a significant part in diagnosing and distinguishing diseases and monitoring these diseases' quality. In Medical Images, detection of breast cancer in its earlier stage is most important in this field. Because of the low contrast and uncertain design of the tumor cells in breast images, it is still challenging to classify breast tumors only by visual testing by the radiologists. Hence, improvement of computer-supported strategies has been introduced for breast cancer identification. This work presents an efficient computer-assisted method for breast cancer classification of digital mammograms using Adaptive Resource Allocation Neural Network (ARAN). At first, breast cancer images were taken as input, preprocessing step is utilized to eliminate the noise and unimportant data from the image utilizing a Butterworth filter. Adaptive histogram equalization is utilized to improve the contrast of the image. Multimodal clustering segmentation has been applied, and Tetrolet transformation based feature extraction is applied at various levels, Based on this, data classification is implemented. For exact classification, ARAN is utilized to predict if the patient is influenced by breast cancer. Compared with other current research techniques, the proposed strategy predicts the results efficiently. The overall accuracy of ARAN-based mammogram classification is 93.3%.

Keywords: Adaptive Resource Allocation Neural Network, Butterworth filter, histogram equalization, breast cancer

1. INTRODUCTION

The leading cause of female deaths in the world is due to breast cancer. It has been observed that early detection of cancer can help to decrease the mortality rate among women, and it can potentially help to increase life expectancy. In breast cancer diagnosis, among the available various techniques, mammography is the most promising technique and used by radiologists frequently. Mammogram images are generally of low contrast and added with noise. On breast mammogram bright areas do not indicate cancer. In some mammograms, there may be malignant tissue and normal dense tissue.

Finding the difference in the contrast between malignant and normal dense tissues is not possible by applying manual identification processing. A mammogram is essential to understand cancerous lesions' mass areas and understand the tumor and its segmentation. Therefore, the detection of malignant lesions in mammogram images is one of the active research areas. Many techniques, including computer-assisted detection systems and machine leaning-based methods, were introduced to segment breast cancer in mammogram images. However, no solution promises the best or can successfully meet the criteria of detecting only cancerous regions.

This work focuses on detecting tumors, representatives of the values of the more intense reference on the breast area. However, in special normal dense tissues with intensities similar to the tumor area, it is necessary to identify the tumor area, excluding these areas successfully. This work consists of four stages: Preprocessing, Segmentation, Feature extraction, and classification.

2. RESEARCH BACKGROUND

Several researchers have been made to show an automatic recognition framework for the early analysis of breast cancer. In [1-3], authors used a Probabilistic Neural Network (PNN) based mammogram classification detailing a precision of 87.66%. In [4, 5] proposed a CAD model using GLCM for feature extraction followed by order utilizing k-NN, SVM [6], and Artificial Neural Network (ANN) [7]. Also, it

consolidates histogram balance, some morphological tasks, and an Otsu's-based thresholding strategy for dividing the ROIs. As referenced, the classifiers' exactness is 73%, 83%, and 77%, individually [8, 9].

A mixture technique using wavelet and curvelet transform was introduced [10, 11] to extract the mammograms' features. In [12-16] used a covering-based strategy for feature choice. This plan used the Fuzzy genetic framework for feature choice and obtained the precision of 89.47%. In [17] proposed two distinctive automated techniques to order the classify the harmful mammogram tissues. The principal segmentation procedure is performed through an automated district developing whose ANN threshold is procured [18]. The resulting segmentation is finished by a Cellular Neural Network (CNN) whose limits are created utilizing a Genetic Algorithm (GA) [19, 20].

At last, extraordinary characterization models like MLP, k-NN, SVM, naıve Bayes, and arbitrary timberland are used, yielding a precision of 86.47% with MLP [21-23]. In [24], proposed a CAD framework to improve the extricated feature set utilizing the Genetical Swarm Optimization (GSO) algorithm in mammograms [25]. In their work, the features are acquired utilizing a Gray-Level Co-Occurrence Matrix (GLCM). It is tracked down that all separated features are not important, and to moderate this, GSO is utilized to advance the Feature Vector (FV). Further, SVM is applied to characterize the mammogram as ordinary or unusual. This methodology yields an exactness of 87%.

Another CAD model using Fast Finite Shearlet Transform (FFST) for feature extraction is created [26]. Here, the extricated FFST features are positioned utilizing the t-test filter. Further, SVM is used on the chosen set of features for classification utilizing MIAS and DDSM datasets. In [27], a micro-calcification (MC) identification procedure was introduced utilizing non-connecting simplified PCNN and reported a significant precision. In [28], an analysis framework was proposed dependent on an Extreme Learning Machine (ELM) to classify the mammograms as benign or malignant with great exactness.

3 ARAN WITH WHITE MASS ESTIMATION FOR IMPROVED MICROCALCIFICATION IDENTIFICATION

Early detection of breast cancer is believed to increase survival. The best available breast imaging technique is to use low dose X-rays to detect breast cancer before experiencing mammography symptoms. Mammograms may indicate breast cancer in a better manner for the people with defects and micro calcifications. This research's main objective is to develop image processing algorithms and increase the accuracy of breast cancer diagnostics in computer-assisted detection by categorizing women into different risk groups. The block diagram of the proposed method is shown in Figure 1.

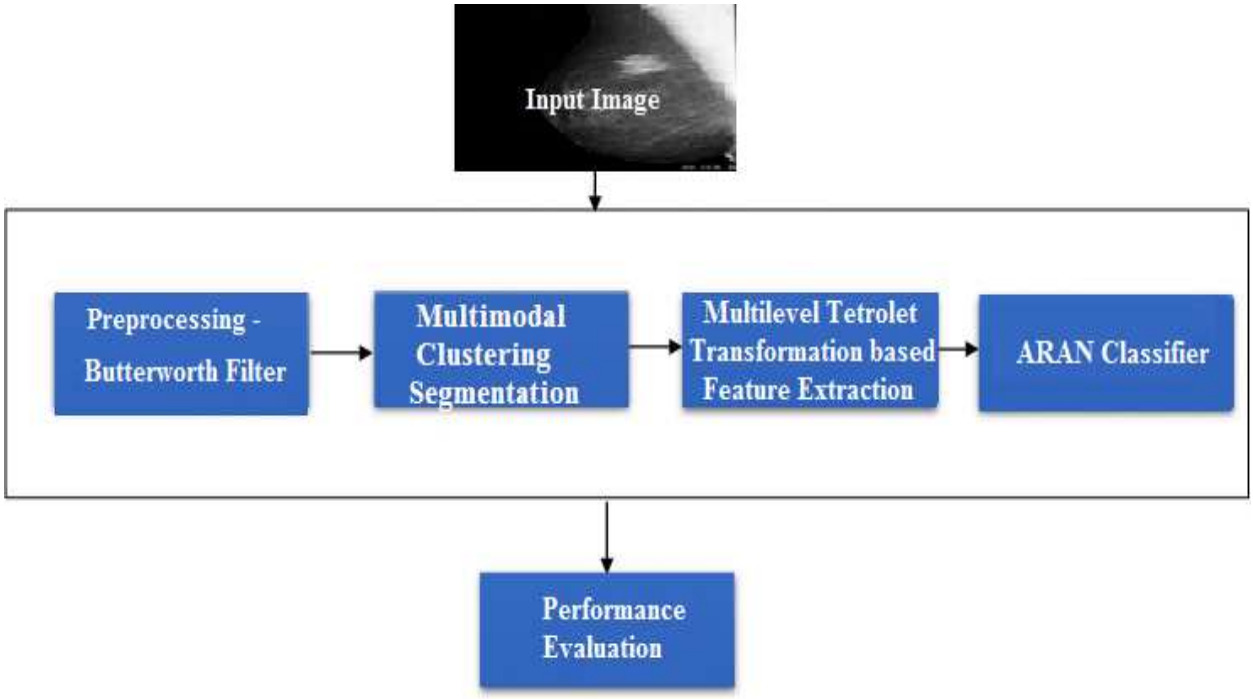

Figure 1 Block Diagram of Proposed System

3.1 PREPROCESSING – BUTTERWORTH FILTER

Usually, digital mammogram images are distorted due to the sensors used and the other artifacts. Therefore, accurate results are not possible. So preprocessing techniques are used to improve images with higher accuracy results. In this work, a preprocessing

method with a Butterworth filter is introduced to enhance the input image. The proposed preprocessing filter is tuned to the local ridgeline direction. The ridge frequency is applied to the channel pixel normalized input mammogram image to obtain an enhanced image.

3.1.1. Butterworth filter Algorithm

Step 1: *Read the input image*

Step 2: *Apply Butterworth low pass filter for smoothing domain correction*

2.1 The transfer function of a Butterworth low pass filter (BLPF) of order n, and with cut-off frequency at a distance D0 from the origin, is defined as equation (1)

$$H(u,v) = \frac{1}{1+[D_o/D(u,v)]^{2n}} \ldots (1)$$

Step 3: *Apply Butterworth High pass filter for sharpening domain correction.*

2.1 The transfer function of Butterworth high pass filter (BHPF) of order n and with cutoff frequency r0 is given by equation (2)

$$L(u,v) = \frac{1}{1+[D(u,v/D_o)]^{2n}} \ldots (2)$$

u, v = References Pixels D_0 *= Cut off frequency*

n = Order of Filter (usually 1-3). *D = Variance of adaptive white Gaussian noise*

Where

D_0 = cut-off frequency of the Butterworth filter, which is the proposed filter order, controls the proposed system's phases. The function of Butterworth filter consists of two domains, such as smoothing domain and sharpening domain

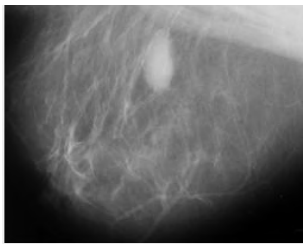

a) Input_image1

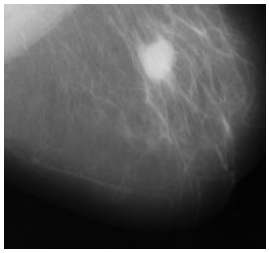

b) Input_image2

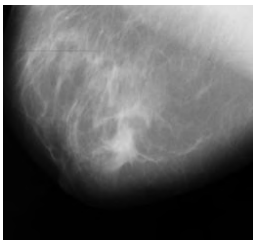

c) Input Image3

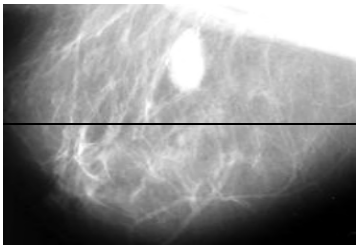

d) Preprocessed_image1

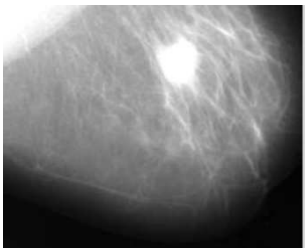

e) Preprocessed_image2

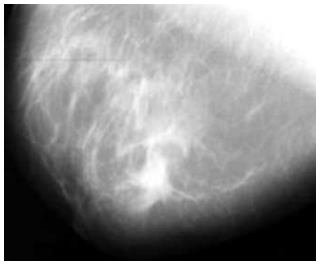

f) Preprocessed_image3

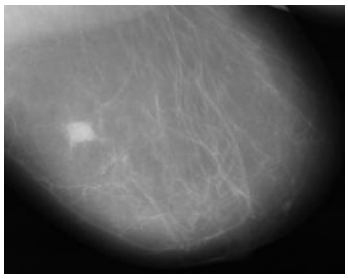

g) Input_image4

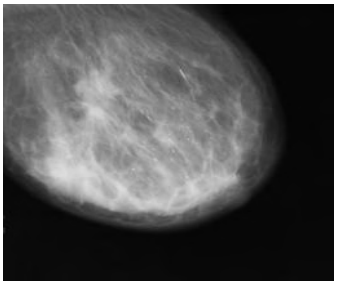

h) Input_image5

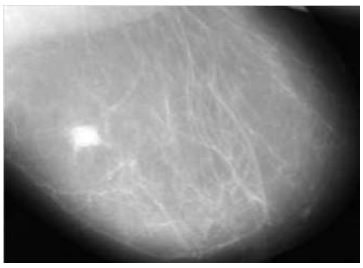

i) Preprocessed_image4

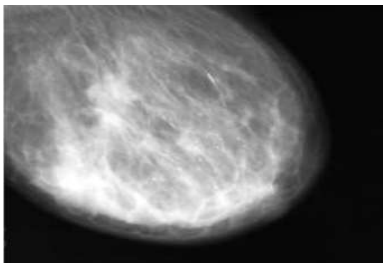

j) Preprocessed_image5

Figure 2 Input Image (DDSM Dataset) and Preprocessed Image

The Result of the Preprocessing is shown in Figure 2. As compared with the input image (Fig.2a, 2b, 2c, 2g and 2h), the preprocessed (Fig.2d, 2e, 2f, 2i and 2j) image have low noise.

3.2 MULTIMODAL CLUSTERING SEGMENTATION

The second stage CAD-based mass detection plan, is to separate suspicious areas that include masses from the background parenchyma, i.e., divide the mammogram into several non-attempted areas and then exclude Region of interest (ROIs) and place suspicious mass region. The suspect area is brighter than its surroundings and has an almost uniform density, the size is varied and has blurred boundaries. Segmenting the mass of a sculpture from others can be a complex process due to the diversity of the mass characteristics from one image to another. In this work, Multimodal clustering segmentation method is used. Multimodal Clustering Segmentation is considered the most important overlooked learning problem. This system finds and collects the unlabeled information. Clustering is the process of organizing objects into groups that are similar in some way to a member.

A cluster is a set of items "similar" among them and "different" from other cluster objects. An iterative system starts relegating every pixel to the closest gathering center utilizing a different measure D (Equation (3)), which consolidates separation of clustering accuracy (Equation (4)) and separation of spatial accuracy (Equation 5).

$$D = \sqrt{\left(\frac{d_c}{m}\right)^2 + \left(\frac{d_s}{S}\right)^2} \quad \ldots. (3)$$

$$d_c = \sqrt{\sum_{S_p \in B} \left(I(x_{i,} y_{i,} S_p) - I(x_{j,} y_{j,} S_p)\right)^2} \ldots . (4)$$

$$d_s = \sqrt{(x_{ij} - y_{ij})^2} \ldots. \quad (5)$$

Where

D = Separation measure

d_c = Clustering Accuracy

I = Number of Iterations

S = Quantity of separated Pixel

x = Set of Pixels

y = Set of cluster centers

In this work, the clustering result is formed from mammogram images for two classes. Each type has a three-dimensional vector character with a gray and black value per pixel along with the class label.

3.2.1 Algorithm Steps of Multimodal Clustering Segmentation

Input: *Preprocessed image*

Output: *Number of Clusters*

Begin

Step 1: *Create and initialize a data structure*

Step 2: *Initialize and compute the centroid for each class*

$$\boldsymbol{C_{ij} = \frac{\sum_{q=0}^{m_i} Dat_{i,j,q}}{m_i} \ldots (6)}$$

Where C_{ij} = centroid, j = number of features, q= number of patterns and i = total number of classes

Step 3: *Calculate the data matrix in every pixel*

3.1 obtain the result of centroid distance in every cluster.

$$Distance = \sqrt{(Pixel\ Data\ matrix - C_{ij})^2} \ldots (7)$$

3.2 calculate the minimum distance and Assign cluster labels

$$Pixel_i = Classlabel(minimum(distance[i]) \ldots (8)$$

Step 4: *Evaluate the objective function*

$$J = \sum_{i=1}^{N} \sum_{j=1}^{C} \mu_{ij} |x_i - C_j|^2 \ldots (9)$$

Where J is the objective function N is the number of pixels in the image, C is the number of clusters, μ is the centroid of xi's cluster, x_i is the i^{th} pixel in N, c_j is j^{th} cluster in C and $|x_i - c_j|$ is the Euclidean distance between xi and c

Step 5: *Move to step 3 and repeat the process until the objective function minimized*

Step 6: *label in the final class is assigned. The result of segmentation is shown in Figure 3.*

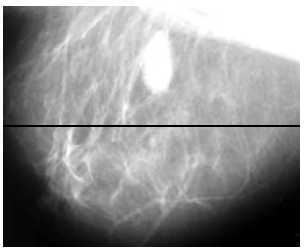

a) Preprocessed_image1

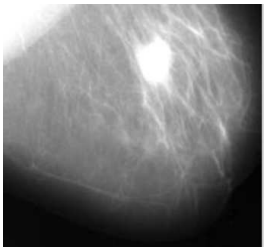

b) Preprocessed_image2

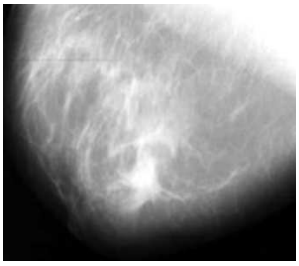

c) Preprocessed_image3

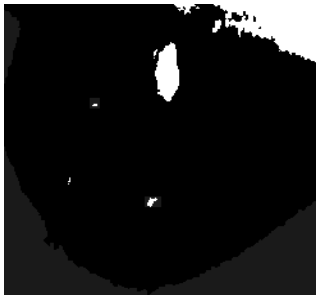

d) Segmented_Image1

e) Segmented_image2

f) Segmented_image3

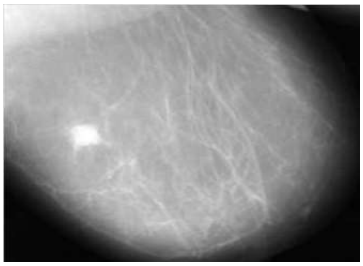

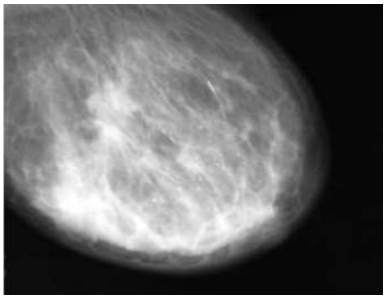

g) Preprocessed_image4 h) Preprocessed_image5

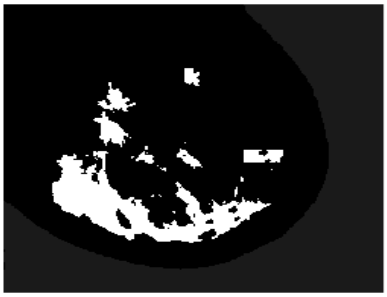

i)Segmented_image4 j) Segmented_image5

Figure 3. Segmentation Output

3.3 MULTILEVEL TETROLET FEATURE EXTRACTION

The extracted feature distribution can specify each pixel of a digitized mammogram, according to their neighboring pixels. Feature extraction in mammogram analysis is practically inevitable, and a good selection of features gives it high accuracy. This feature values the image, which is called the feature vector helps in finding the abnormality. The Multilevel Tetrolet Transformation based Feature extraction method is used to extract the mammogram's features in this work.

Table 1: Feature Extraction Results for various samples

Features	**Result of Sample 1**	**Result of Sample 2**	**Result of Sample 3**	**Result of Sample 4**	**Result of Sample 5**
Mean	0.0041	0.0040	0.0049	0.0018	0.0044

Standard Deviation	0.0918	0.0896	0.0995	0.0994	0.0991
Entropy	3.383	2.7748	2.3296	2.8915	2.1061
RMS	0.09	0.08986	0.0987	0.0996	0.0995
Variance	0.093	0.0088	0.0088	0.0087	0.0085
Smoothness	0.9346	0.9316	0.9452	0.8429	0.9389
Kurtosis	13.041	13.5562	11.8532	9.2515	13.1218
Skewness	1.187	1.3942	1.0831	0.6812	1.1021
IDM	0.572	1.10642	0.13572	0.4313	0.2136
Contrast	0.2775	0.3232	0.2711	0.2391	0.2925
correlation	0.1058	0.1534	0.01847	0.2061	0.17743
Energy	0.789	0.7632	0.7675	0.7915	0.8043
Homogeneity	0.948	0.9345	0.9389	0.9578	0.9963

After retrieving the segmented region features, the tumor region has been classified by applying the adaptive resource allocation neural network classifier. The function of the adaptive resource allocation neural network classifier is discussed in the following section.

3.4 Adaptive Resource allocation Neural network Classifier

Adaptive Resource Allocation Network (ARAN) classifiers are trained feed-forward network type using supervised training algorithms. The ARAN network's main

advantage is that it uses only a single hidden layer and uses the radial basis function as its execution function. The ARAN network usually trains much faster than back-propagation systems. This network is less suspected of problems because of the behavior of the non-standard input in hidden units. The following equation 10 shows the overall network output of ARAN.

$$y(x) = \sum_{i=1}^{M} w_i \, e^{\left(\frac{-(|x-c_i)^2}{2\sigma^2}\right)} \quad \ldots (10)$$

Where

x, y(x) = input and output function c_i = Cluster center

σ = Center basis function M = number of basis function centered.

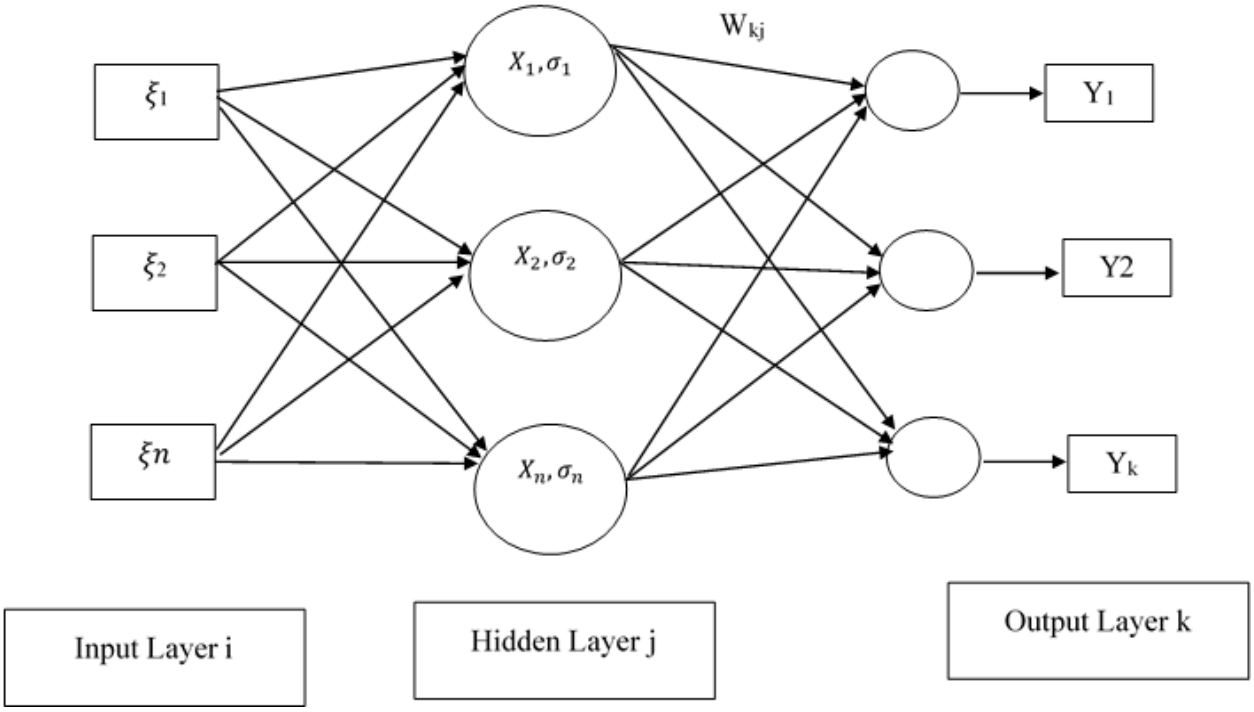

Figure 4. Architecture of ARAN

Adaptive Resource Allocation Network is a type of sequential learning-based Radial Basis Function (RBF) network. Thus ARAN is a network that learning new computational units that allocate more patterns. The center (X_j) and a width (σ_j) are two important parameters associated with each hidden unit. The activation function of each hidden unit is symmetric to the input space. The output of every hidden unit depends

only on the radial distance between the input vector ξ_i and the hidden unit X_j parameter center. The weight of every hidden unit and output unit are connected using W_{kj}.

The following equations discuss the overall network output.

$$O_k = \sum_j W_{kj} V_j \ , j = 1 \text{ to n (number of hidden units)} \ \ldots (11)$$

$$V_j = e^{-|X_j - \xi_i|^2 / 2_j^{\sigma^2}} \ \ldots (12)$$

Where

V_j = j^{th} hidden unit's Result W_{kj} = Weight connect between hidden unit j and output k X_j =Center σ_j = width of hidden unit

The learning period of ARAN includes the portion of new hidden units and the variation of network boundaries. The network starts with no hidden units, i.e., the network begins with no data's and no patterns are yet stored. As input-output (ξ_i, y_k) information are gotten during training, some of them are utilized for creating new hidden units relies upon the information which is chosen the accompanying conditions

$$d = \left|X_j - \xi_i\right| > \delta \ \ldots (13)$$

$$e = |y_k - O_k| > e_{min} \ \ldots (14)$$

Where

X_j = Center, which is neared to ξ_i

δ and e_{min} = Thresholds value of width and center

If the above two conditions are fulfilled, the information is viewed as unique, and another hidden unit is added. The principal level expresses that the information should be at a distance from all centers, and the subsequent condition expresses that the error between the network output and the target output must be significant.

The e_{min} addresses the ideal approximate accuracy of the network output, and the δ addresses the distance in resolution size of the input space. The network begins with $\delta_n = \delta_{max}$. The estimation of δ_{max} as the enormous interest in this info space, normally the whole non-resident input space is picked with zero probability. The distance δ is mathematically disintegrated as δ =max $\{ \delta_{max}, \gamma^n , \delta_{min}\}$,, where $0 < \gamma < 1$ is the decay

constant. The value for δ is decomposed until δ_{min}, where it reaches the smallest length scale of interest.

The exponential decaying of the norm allows far less basic tasks with larger widths. With the number of observations, the smaller widths' functions are fine-tuned to separate the approximation. The following equations give the parameters with the new hidden unit.

$$W_{kj}(new) = e \ldots (15)$$

$$X_j(new) = X_j \ldots (16)$$

$$\sigma_j(new) = k|X_j - \xi_i| \ldots (17)$$

Where

k = overlap factor determines the overlap of the hidden units' responses in the input space. As k grows more extensive, the reactions of the units overlap more and more.

When an observation (ξ_i, y_k) is not pass new criteria, and a new hidden unit is not added. But the network parameters can only be adapted to match the X_j and W_{jk} observation. The Least Mean Squared (LMS) algorithm is used to adjusting the X_j and W_{jk}. The ARAN algorithm is discussed as follows

Algorithm Steps of ARAN

Step 1: *Set* $\delta = \delta_{max}$

Step 2: *For a given pair of input-output* (ξ_i, y_k)*, Compute the output* $O_k = \sum_j W_{kj} V_j \ , j = 1 \ to \ n$

Step3*: Compute the error* $e = y_k - O_k$

Step 4: *Compute* $\delta = max\{ \delta_{max}, \gamma^n , \delta_{min}\}$,

Step 5*:* ***If*** $d > \delta$ *and* $e > e_{min}$*, then insert a Radial Bias Function unit into the hidden layer,*

set its width $\sigma_j = k|X_j - \xi_i|$ *and set the center coordinates equal to input pattern*

K = overlap factor that determines the amount of overlap of the responses of the hidden units in the input space

Else

Step 6: *Update the weights using the following equations*

$$W_{kj}(new) = W_{kj}(old) + \alpha * e * V_j \text{ Where } \alpha \text{ is learning Rate}$$

$$X_{ji}(new) = X_{ij}(old) + \Delta X_{ji}$$

Where

$$\Delta X_{ji} = \frac{2\eta}{\sigma^2} * (X_j - \xi_i) * V_j * \sum (O_k - y_k) * W_{kj}$$

Step 7*: Save the network parameters and classify the result of mammogram*

Accuracy, specificity and sensitivity are utilized to assess the proposed Adaptive resource allocation neural network framework. These parameters are estimated through MatLab simulation. The explanation and mathematical formulation about accuracy, sensitivity and specificity are given below.

$$\text{Sensitivity} = \frac{T_p}{T_p + F_n} * 100 \quad (18)$$

The Specificity is termed as a negative probability for the image test, and it can be estimated by Equation (19)

$$\text{Specificity} = \frac{T_n}{T_n + F_p} * 100 \quad (19)$$

Accuracy is the probability that an imaging test is performed correctly. It is then found by Equation (20)

$$\text{Accuracy} = \frac{T_p + T_n}{T_p + T_n + F_P + F_n} * 100 \quad (20)$$

Where

T_p = *True positive* T_n = *True negative*

F_p = *false positive* F_n = *False negative*

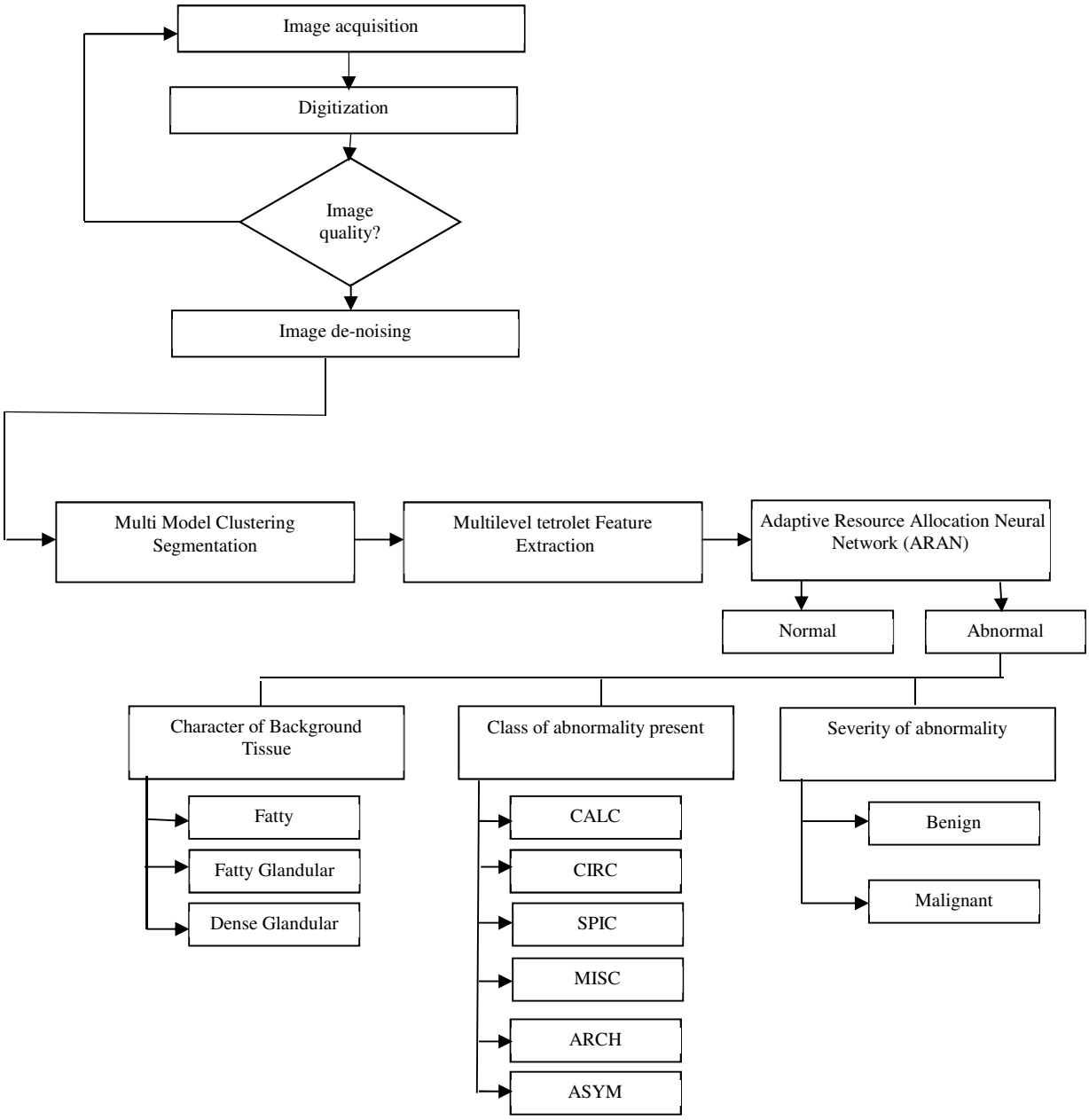

Figure 5 Flow Chart of Proposed ARAN based Mammogram Classification

The overall flow chart of the proposed ARAN is shown in Figure 5. Accessed from the exclusive image features, this method can distinguish pixels that respect themselves on a low resolution scale. The technology selects a small pixel arrangement with the microcalcification to determine the pixel that exceeds the clear edge self-esteem light. Based on the number of distinguished pixels and the area's span, the proposed system dealing with microcalcification depth measures. The comparability of small-scale calcifications is registered by the similarity of the more in-depth actions of smaller-scale calcifications. Each segment has its small-scale calcification depth

measure given the deep microcalcification measures, the comparability with other areas in this work process.

4 SIMULATION RESULTS AND DISCUSSION

This section discusses the simulation results and performance analysis of the proposed Adaptive Resource Allocation Neural Network-based mammogram classification system. For evaluation, the DDSM and MIAS data set have been used. The details of datasets are shown in Table 1, and the GUI screen of the proposed system is shown in Figure 6

Table 1: Details of Dataset

Dataset	***Category***	***Number of images***
MIAS	*Normal (Class-1)*	*200*
	Benign (Class-2)	*68*
	Malignant (Class-3)	*54*
DDSM	*Normal (Class-1)*	*164*
	Benign (Class-2)	*640*
	Malignant (Class-3)	*760*
TOTAL		*1887*

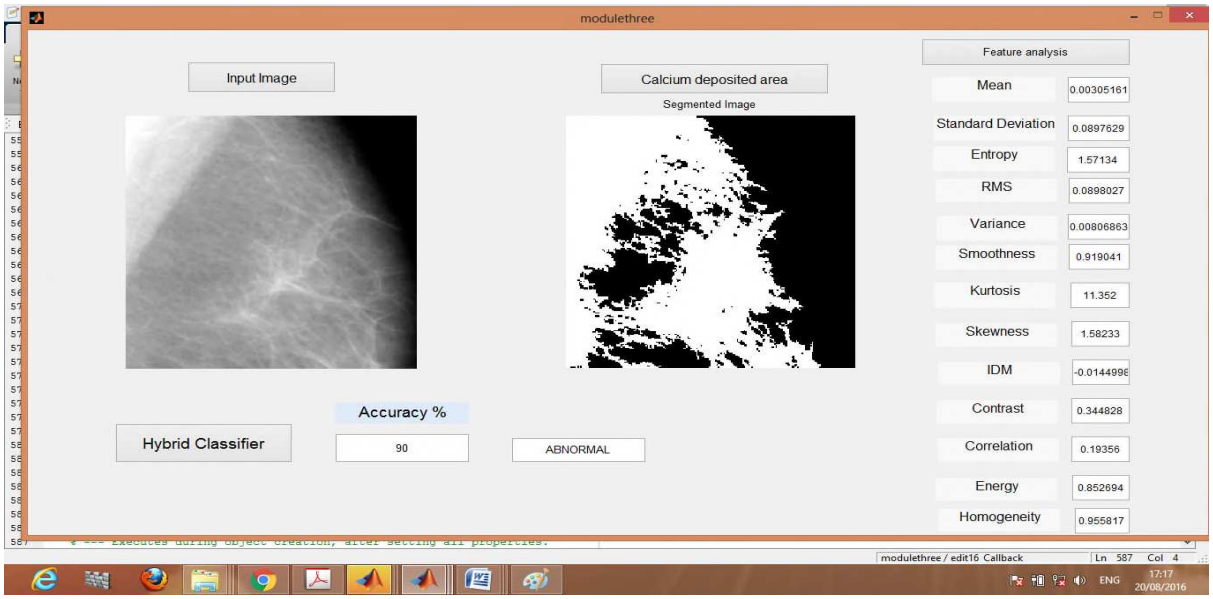

Figure 6 GUI Screen of Proposed System

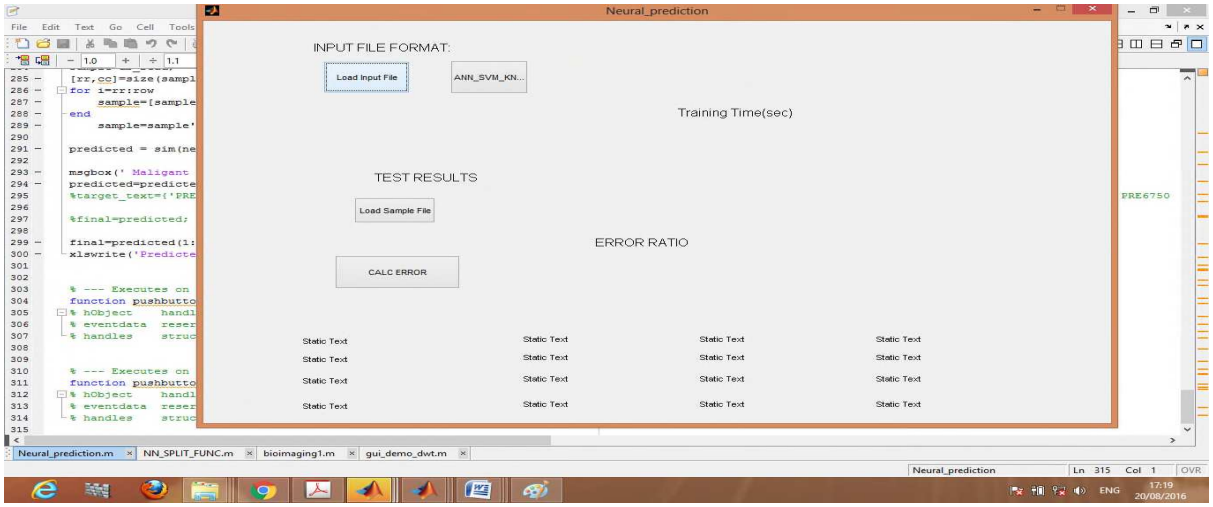

Figure 7 Input Data training

The simulation result screenshot of input data training and error ratio evaluation of the proposed adaptive resource allocation neural network-based mammogram classification system is shown in Figure 7.

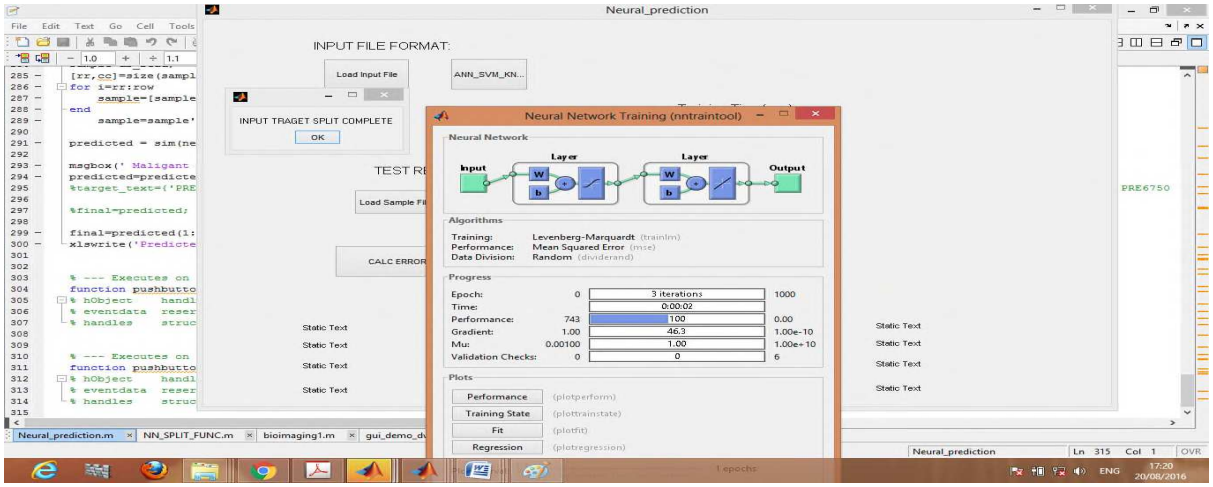

Figure 8 Simulation Result of weight adjustment

The simulation result screenshot of input data training weight adjustment of proposed adaptive resource allocation neural network-based mammogram classification system is shown in Figure 8.

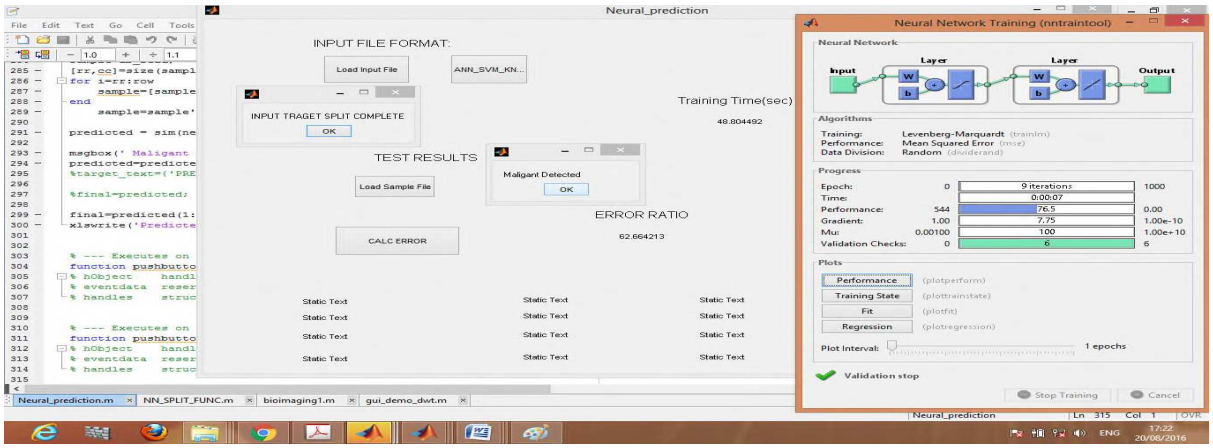

Figure 9 GUI Screen of Testing

The simulation result screenshot of input test data with weight adjustment of proposed adaptive resource allocation neural network-based mammogram classification system is shown in Figure 9.

Figure 10 Simulation result with abnormality classification

The simulation result screenshot of abnormality classification of the proposed adaptive resource allocation neural network-based mammogram classification system is shown in Figure 10. The following Class of abnormality is present: Calcification (CALC), Well-defined/circumscribed masses (CIRC), Spiculated masses (SPIC), ill-defined masses (MISC), Architectural distortion (ARCH), Asymmetry (ASYM) and Normal (NORM)

Table 2 Confusion Matrix of Class-1 for MIAS Dataset for ARAN

	Positive	***Negative***
Positive	*True Positive =98*	*False Positive = 2*
Negative	*False Negative =8*	*True Negative=92*

Table 3 Confusion Matrix of Class-1 for DDSM Dataset for ARAN

	Positive	***Negative***
Positive	*True Positive =78*	*False Positive = 2*
Negative	*False Negative =8*	*True Negative=73*

Tables 2 and 3 discuss the confusion matrix's simulation results for class-1 in MIAS and DDSM datasets with Adaptive Resource allocation neural networks. The result of this class-1 confusion matrix is used to evaluate the performance of the proposed system.

Table 4 Performance analysis of ARAN with Class-1 data's

Evaluation Parameters	*Result of Class-1 for MIAS Dataset*	*Result of Class-1 for DDSM Dataset*
Sensitivity (%)	*92.45*	*90.69*
Specificity (%)	*97.87*	*97.33*
Accuracy (%)	*95.0*	*93.78*

The performance analysis of the proposed Adaptive Resource allocation neural network-based class-1 mammogram classification system of MIAS and DDSM dataset is shown in Table 4. Based on the value of table 4, the graphical analysis result is discussed in figure 11.

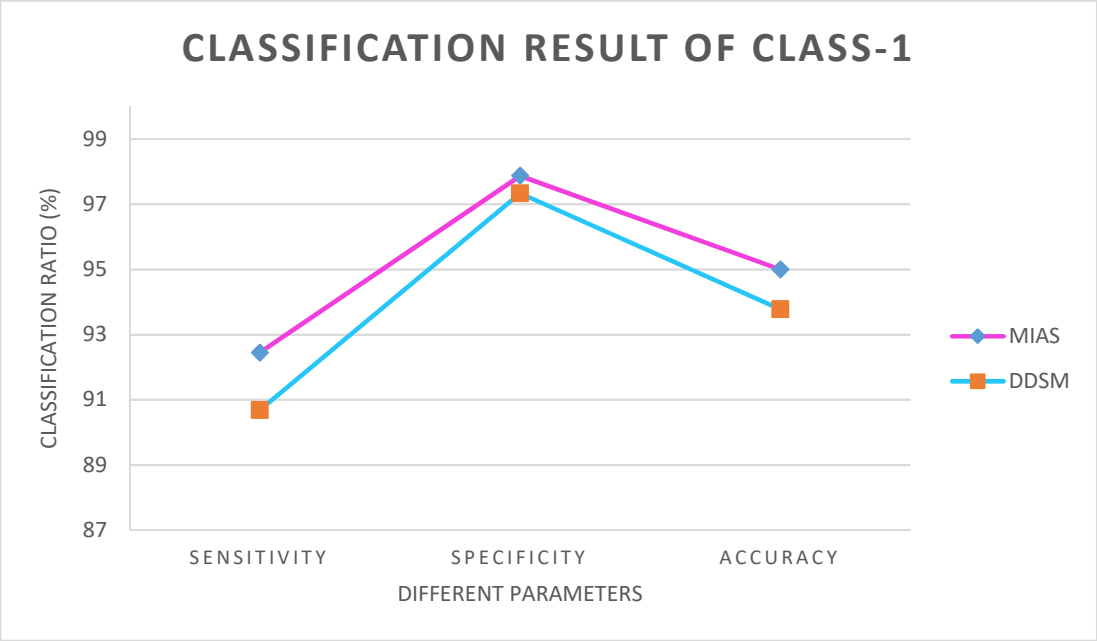

Figure 11 Classification Result of Class-1

The classification result of class-1 for the MIAS and DDSM dataset is shown in Figure 11. The proposed ARAN classifier perfectly classify the result of class-1. The sensitivity, specificity and accuracy of Proposed ARAN with MIAS dataset's class-1 results are 92.45%, 97.87% and 95.0%, respectively. The sensitivity, specificity and accuracy of Proposed ARAN with the DDSM dataset's class-1 results are 90.69%, 97.33% and 93.78%, respectively.

Table 5 Confusion Matrix of Class-2 for MIAS Dataset

	Positive	***Negative***
Positive	*True Positive =30*	*False Positive = 2*
Negative	*False Negative =5*	*True Negative=31*

Table 6 Confusion Matrix of Class-2 for DDSM Dataset

	Positive	***Negative***
Positive	*True Positive = 298*	*False Positive =8*
Negative	*False Negative =27*	*True Negative= 307*

Tables 5 and 6 discuss the confusion matrix's simulation results for class-2 in MIAS and DDSM datasets, respectively. The result of this class-2 confusion matrix is used to evaluate the performance of the proposed system. The Performance analysis of ARAN with Class-2 data is shown in Table 7.

Table 7. Performance analysis of ARAN with Class-2 data's

Evaluation Parameters	*Result of Class-2 for MIAS Dataset*	*Result of Class-2 for DDSM Dataset*

Sensitivity (%)	*88.23*	*91.69*
Specificity (%)	*96.87*	*97.46*
Accuracy (%)	*92.42*	*94.53*

The performance analysis of the proposed Adaptive Resource Allocation Neural Network-based class-2 mammogram classification system of MIAS and DDSM dataset is shown in Table 7. Based on the value of table 7, the graphical analysis result is discussed in figure 12.

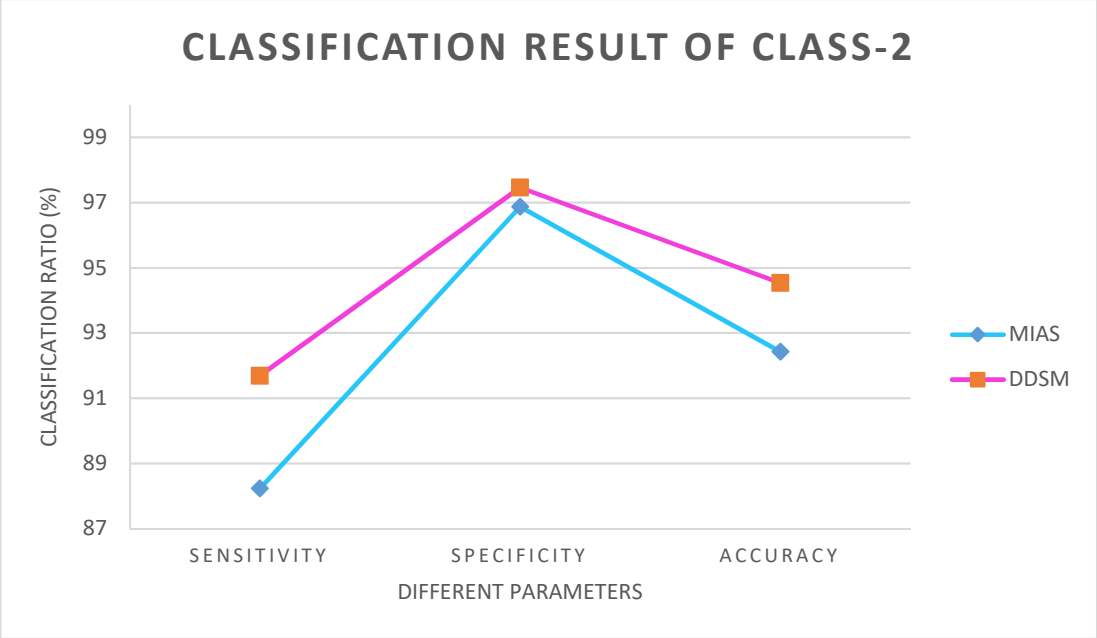

Figure 12 Classification Result of Class-2

The classification result of class-2 for the MIAS and DDSM dataset is shown in Figure 12. The proposed ARAN classifier perfectly classify the result of class-2. The sensitivity, specificity and accuracy of Proposed ARAN with MIAS dataset's class-2 results are 88.23%, 96.87% and 92.42%. The sensitivity, specificity and accuracy of Proposed ARAN with DDSM dataset's class-2 results are 91.69%, 97.46% and 94.53%, respectively.

Table 8 Confusion Matrix of Class-3 for MIAS Dataset

	Positive	***Negative***
Positive	*True Positive =26*	*False Positive = 1*
Negative	*False Negative =3*	*True Negative=24*

Table 9 Confusion Matrix of Class-3 for DDSM Dataset

	Positive	***Negative***
Positive	*True Positive =350*	*False Positive = 14*
Negative	*False Negative =31*	*True Negative=365*

Tables 8 and 9 discuss the confusion matrix's simulation results for class-3 in MIAS and DDSM datasets. The result of this class-3 confusion matrix is used to evaluate the performance of the proposed system. The Performance analysis of ARAN with Class-3 data is shown in Table 10.

Table 10 Performance analysis of ARAN with Class-3 data's

Evaluation Parameters	*Result of Class-1 for MIAS Dataset*	*Result of Class-1 for DDSM Dataset*
Sensitivity (%)	*89.65*	*91.86*
Specificity (%)	*96.0*	*96.30*
Accuracy (%)	*92.59*	*94.07*

The performance analysis of the proposed Adaptive Resource Allocation Neural Network-based class-3 mammogram classification system of MIAS and DDSM dataset

is shown in Table 10. Based on the value of table 10, the graphical analysis result is discussed in figure 13

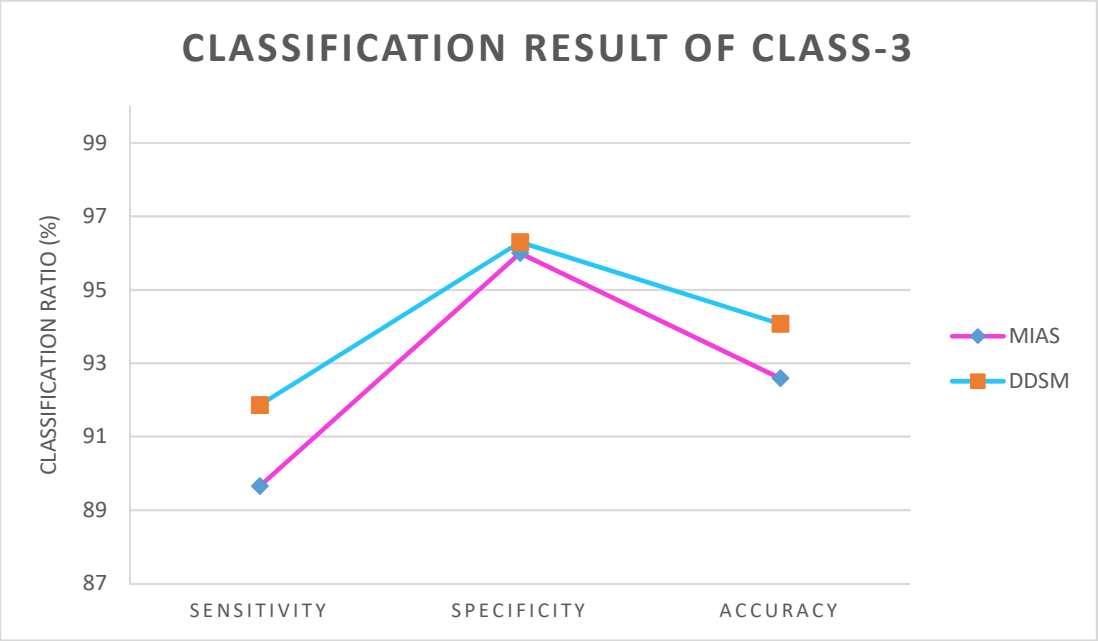

Figure 13 Classification Result of Class-3

The classification result of class-3 for the MIAS and DDSM dataset is shown in Figure 13. The proposed ARAN classifier perfectly classify the result of class-3. The sensitivity, specificity and accuracy of Proposed ARAN with MIAS dataset's class-3 results are 89.65%, 96.0% and 92.59%. The sensitivity, specificity and accuracy of Proposed ARAN with DDSM dataset's class-3 results are 91.86%, 96.30% and 94.07%, respectively.

Table 11 Performance evaluation of Overall Classification Accuracy with different classifiers

Sl.No	***Name of the Researcher & year***	***Techniques used***	***Database***	***Overall Classification Accuracy***
1	*Y. Ireaneus Anna Rejaniet et al., 2009*	*SWT, Shape features SVM(RBF kernel)*	*MIAS*	*88.75%*

3	*Ioan B. et al. 2011*	*Gabor wavelets and directional features, Feature reduction using PCA, SVM*	*MIAS*	*84.37%*
4	*P.Valarmathi 2018*	*Texture features, shape features, margin features-SVM (RBF)*	*MIAS*	*82.30%*
7	*Proposed Work*	*MLTT-Texture features -ARAN*	*MIAS*	*93.33*

Table 11 discusses the proposed ARAN method's overall classification ratio analysis with some other existing processes with the MIAS dataset. As compared with existing SVM and PCA methods, the proposed methods achieve the best classification accuracy. The overall accuracy of ARAN-based mammogram classification is 93.33%.

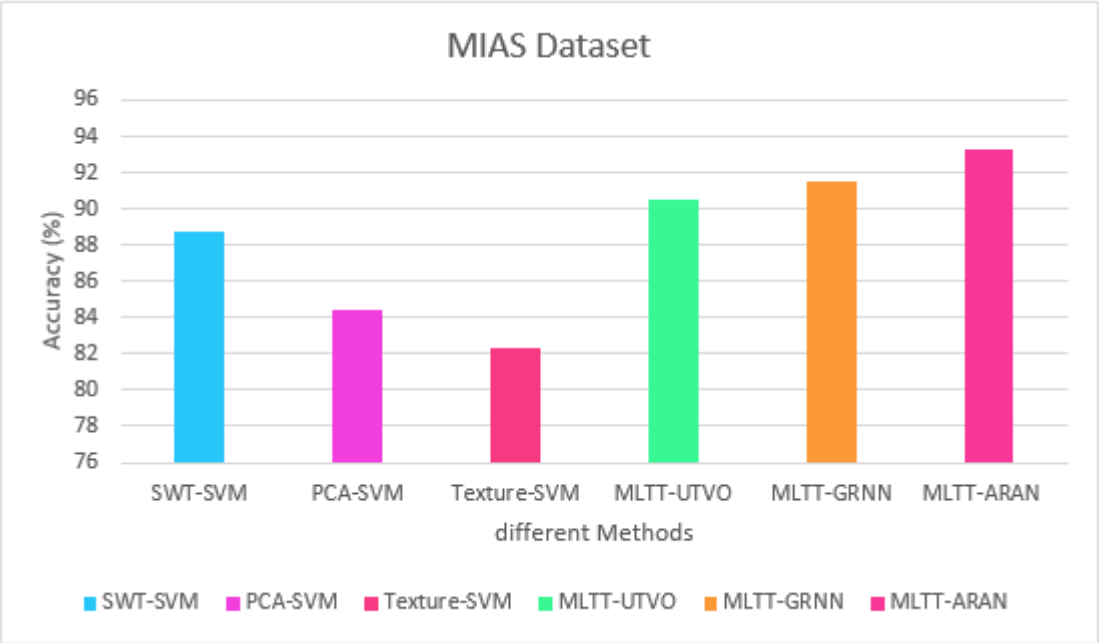

Figure 14 Overall classification Ratio analysis-ARAN

Figure 14 discusses the overall classification ratio accuracy analysis of the proposed method with some other existing methods. As compared with existing methods, the proposed ARAN gives the best result against the MIAS dataset. The overall accuracy of ARAN-based mammogram classification is 93.33%.

4. CONCLUSION

This work demonstrates how neural networks are used to detect, segment, and classify mammograms being expressed. Using the centers and widths of the hidden nodes as templates for detection and segmentation provides a guide for intelligent search through possible mammogram space. This approach increases cancer detection by collecting the desired specific objects to submit a request; improving segmentation by generating high-quality initial outlines with different objects. The centers and widths are relatively new using the Adaptive Resource Allocation Neural Network to creating a tight set and well-separated clusters. The system supports a clear screen hidden in nodes as templates. The simulation results demonstrate that the proposed method's learning rate is good. The overall sensitivity, specificity and accuracy of the MIAS-based dataset are 90.11%, 96.91% and 93.33%. The overall sensitivity, specificity and accuracy of DDSM based dataset are 91.41%, 97.03% and 94.10%, respectively. Further directions of this work shall include a deep learning method to improve the performance and reduce the computational complexity.

1. Availability of data

   Data availability

   Using dataset in this paper DDSM

2. Declaration statements

The optimizer and activation function in Adaptive Resource Allocation Neural Network declare that they have no consent.

3. Funding

   No funding

4. Conflicts of interest

No conflict of interest

5. Authors' contributions

Based on the classification results produced the Adaptive Resource Allocation Neural Network is taken to build the crop recommendation model.

REFERENCES

1. Zhao, Y., Chen, D., Xie, H., Zhang, S. & Gu, L. Mammographic image classification system via active learning. J. Med. Biol. Eng. 39, 569–582 (2019).
2. Voulodimos, A., Doulamis, N., Doulamis, A. & Protopapadakis, E. Deep learning for computer vision: A brief review. Comput. Intelligence Neuroscience 20, 18. https://doi.org/10.1155/2018/7068349 (2018).
3. Yu, X., Yu, Z., Wu, L., Pang, W. & Lin, C. Data-driven two-layer visual dictionary structure learning. J. Electron. Imaging 28, 023006 (2019).
4. Che, D. et al. Tire tread pattern recognition based on non-linear activated aggregation residual neural network. J. Jiangxi Univ. Sci. Technol. 40, 80–85 (2019).
5. Yu, X. et al. Deep ensemble learning for human action recognition in still images. Complexity https://doi.org/10.1155/2020/94286 12 (2020).
6. Yang, G. et al. Research on deep learning classifcation for nonlinear activation function. J. Jiangxi Univ. Sci. Technol. 39, 76–83 (2018).
7. Wang, J. et al. Discrimination of breast cancer with microcalcifcations on mammography by deep learning. Sci. reports 6, 1–9 (2016).
8. Huynh, B. Q., Li, H. & Giger, M. L. Digital mammographic tumor classifcation using transfer learning from deep convolutional neural networks. J. Med. Imaging 3, 034501 (2016).
9. Li, B., Ge, Y., Zhao, Y., Guan, E. & Yan, W. Benign and malignant mammographic image classifcation based on convolutional neural networks. In Proceedings of the 2018 10th International Conference on Machine Learning and Computing, 247–251 (2018).

10. Lévy, D. & Jain, A. Breast mass classifcation from mammograms using deep convolutional neural networks. arXiv preprint arXiv :1612.00542 (2016).
11. Cai, H. et al. Breast microcalcifcation diagnosis using deep convolutional neural network from digital mammograms. Comput. Math. Methods Med. 1, 4. https://doi.org/10.1155/2019/2717454 (2019).
12. Maaten, L. V. D. & Hinton, G. Visualizing data using t-sne. J. Mach. Learn. Res. 9, 2579–2605 (2008).
13. Jenifer, S., Parasuraman, S. & Kadirvelu, A. Contrast enhancement and brightness preserving of digital mammograms using fuzzy clipped contrast-limited adaptive histogram equalization algorithm. Appl. Sof Comput. 42, 167–177 (2016).
14. Simonyan, K. & Zisserman, A. Very deep convolutional networks for large-scale image recognition. arXiv preprint arXiv:1409.1556 (2014).
15. Szegedy, C. et al. Going deeper with convolutions. In Proceedings of the IEEE conference on computer vision and pattern recognition, 1–9 (2015).
16. Sivic, J. & Zisserman, A. Video google: A text retrieval approach to object matching in videos. In null, 1470 (IEEE, 2003). 25. Upadhyay, P. K. & Chandra, S. Salient bag of feature for skin lesion recognition. Int. J. Perform. Eng. 15, 1083–1093 (2019).
17. Huang, J.-B. & Yang, M.-H. Fast sparse representation with prototypes. In 2010 IEEE Computer Society Conference on Computer Vision and Pattern Recognition, 3618–3625 (IEEE, 2010).
18. Liu, Y., Chen, X., Ward, R. K. & Wang, Z. J. Image fusion with convolutional sparse representation. IEEE Signal Process. Lett. 23, 1882–1886 (2016).
19. Khan, S., Hussain, M., Aboalsamh, H. & Bebis, G. A comparison of diferent gabor feature extraction approaches for mass classifcation in mammography. Multimed. Tools Appl. 76, 33–57 (2017).
20. Huang, G., Liu, Z., Van Der Maaten, L. & Weinberger, K. Q. Densely connected convolutional networks. In Proceedings of the IEEE conference on computer vision and pattern recognition, 4700–4708 (2017).

21. V. K. Singh, S. Romani, H. A. Rashwan, F. Akram, N. Pandey, and M. Sarker, “Conditional generative adversarial and convolutional networks for X-ray breast mass segmentation and shape classification,”in Proceedings of the Medical Image Computing and Computer Assisted Intervention; MICCAI'18, pp. 833–840, Granada, Spain, 2018.
22. V. Agarwal and C. Carson, “Using deep convolutional neural networks to predict semantic features of lesions in mammograms,” 2015, http://cs231n.stanford.edu/reports/2015/pdfs/ vibhua_final_report.pdf.
23. F. Gao, T. Wu, J. Li et al., “SD-CNN: a shallow-deep CNN for improved breast cancer diagnosis,” Computerized Medical Imaging and Graphics, vol. 70, pp. 53–62, 2018.
24. Y. B. Hagos, A. G. Mérida, and J. Teuwen, “Improving breast cancer detection using symmetry information with deep learning,” in Proceedings of the Image Analysis for Moving Organ, Breast, and Thoracic Images; RAMBO'18, pp. 90–97, Granada, Spain, 2018.
25. G. Valvano, G. Santini, N. Martini et al.,“Convolutional neural networks for the segmentation of microcalcification in mammography imaging,” Journal of Healthcare Engineering, vol. 2019, Article ID 9360941, 9 pages, 2019
26. J.-Z. Cheng, D. Ni, Y.-H. Chou et al., “Computer-aided diagnosis with deep learning architecture: applications to breast lesions in US images and pulmonary nodules in CT scans,” Scientific Reports, vol. 6, no. 1, article 24454, 2016.
27. H. C. Shin, H. R. Roth, M. Gao et al., “Deep convolutional neural networks for computer-aided detection: CNN architectures, dataset characteristics and transfer learning,” IEEE Transactions on Medical Imaging, vol. 35, no. 5, pp. 1285–1298, 2016.
28. C. K. Shie, C. H. Chuang, C. N. Chou, M. H. Wu, and E. Y. Chang, “Transfer representation learning for medical image analysis,” in 2015 37th Annual International Conference of the IEEE Engineering in Medicine and Biology Society (EMBC);, pp. 711–714, Milan, Italy, 2015.